**AALBORG
UNIVERSITY**

# Evaluation of carrier-based control strategies for balancing the thermal stress of a hybrid SiC ANPC converter

Novak, Mateja; Ferreira, Victor; Blaabjerg, Frede; Liserre, Marco

# Evaluation of carrier-based control strategies for balancing the thermal stress of a hybrid SiC ANPC converter

Mateja Novak
*Energy Technology Department*
*Aalborg University*
Aalborg, Denmark
nov@et.aau.dk

Victor Ferreira
*Chair of Power Electronics*
*Kiel University*
Kiel, Germany
vf@tf.uni-kiel.de

Frede Blaabjerg
*Energy Technology Department*
*Aalborg University*
Aalborg, Denmark
fbl@et.aau.dk

Marco Liserre
*Chair of Power Electronics*
*Kiel University*
Kiel, Germany
ml@tf.uni-kiel.de

*Abstract*—SiC devices have recently been demonstrated and utilized in many different multilevel topologies. Active neutral point clamped (ANPC) converter is one of those topologies, where the use of SiC devices can significantly increase the converter power density and reduce the output filter size. In order to achieve this, the control algorithm needs to be tailored to utilize the advantages of each power device technology. Therefore, the control strategies which could produce the optimum results for Si based ANPC might not be the optimum choice for hybrid configuration, where Si and SiC devices are mixed. In this paper, it is presented how different pulse-width-modulation (PWM) based algorithms, originally proposed for Si ANPC converters, affect the loss and junction temperature distribution of a hybrid ANPC converter. The analysis includes the inverter and rectifier operation mode, as well as a high and low modulation index operation. The device junction temperatures distribution is verified using an open module 3-level hybrid ANPC prototype.

*Index Terms*—Active Neutral Point Clamped converter (ANPC), carrier based modulation, hybrid power stage, multilevel converter, SiC, thermal distribution

## I. INTRODUCTION

Multilevel topologies like neutral point clamped converters suffer from unbalanced thermal stress distribution i.e. some devices are utilized more often and thus have to endure very high switching stress [1], [2]. One of the solutions, which can mitigate the aforementioned problem, is the introduction of SiC MOSFETs in the converter topology like demonstrated for hybrid ANPC (H-ANPC) converter in [3]. SiC MOSFETs have reduced switching losses compared to IGBT Si devices, therefore they will operate with a lower temperature.

Depending on which switching frequency the devices are operated and between which devices the commutations occur in the control strategy, there are big differences in the distribution of losses. This can be seen for a full SiC ANPC like in [4] and for full Si ANPC in [5]. For a H-ANPC, where a mix of different device technologies is used, this will have an even larger effect on the stress distribution. Therefore, the control algorithm needs to be adapted to correctly utilize
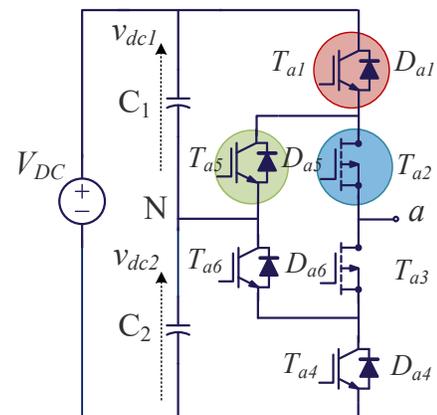
Fig. 1: One phase leg of the H-ANPC converter with SiC MOSFETs ($T_{a2}, T_{a3}$) as inner devices.

the advantages of the SiC devices. In recent publications, the effects of different modulation strategies on the stress distribution, with the most focus on the efficiency, have been analysed in [6]–[10]. From a comparison performed in [6] it can be noticed that for different hybrid configurations the choice of modulation strategy will influence the efficiency of the converter and the thermal stress distribution characteristics. The authors in [10] focus on the development of a PWM method that can reduce the commutation loops and losses in a 4-device SiC ANPC. In [8] a modulation strategy that can efficiently utilize the advantages of the SiC devices to reduce the losses of a 5-level H-ANPC is proposed. However, it needs to be mentioned that most of these publications focus only on one operational point of the converter and they use discrete devices. Applications like motor drives or energy storage systems will typically also require a reverse power flow or operation under lower modulation index. Thus, before selecting the control algorithm for the hybrid topology these operating points also need to be analysed.

In this paper focus will be on the H-ANPC topology with two SiC MOSFETs as the inner devices like shown in Fig. 1. This device configuration showed higher efficiency and
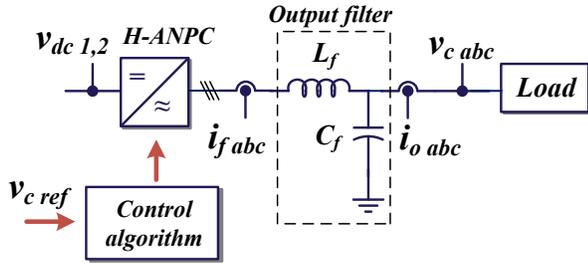
Fig. 2: Schematics of the 3-phase converter system configuration.

TABLE I: Switching states of the three level ANPC converter.

| State | $T_1$ | $T_2$ | $T_3$ | $T_4$ | $T_5$ | $T_6$ |
|-------|-------|-------|-------|-------|-------|-------|
| p1 | 1 | 1 | 0 | 0 | 0 | 1 |
| p2 | 1 | 1 | 0 | 0 | 0 | 0 |
| 0L1 | 1 | 0 | 1 | 0 | 0 | 1 |
| 0L2 | 0 | 0 | 1 | 0 | 0 | 1 |
| 0U1 | 0 | 1 | 0 | 1 | 1 | 0 |
| 0U2 | 0 | 1 | 0 | 0 | 1 | 0 |
| n1 | 0 | 0 | 1 | 1 | 1 | 0 |
| n2 | 0 | 0 | 1 | 1 | 0 | 0 |

lower cost than a four SiC device H-ANPC discussed in [6]. However, the thermal balance characteristics of the two SiC device H-ANPC is not optimal. By finding a control algorithm that could improve the thermal unbalance, this disadvantage could be removed. Therefore, a comparison of four different modulation strategies will be performed in this paper: PWM2 and PWM3 from [11], loss balancing control, which utilizes a temperature feedback [1] and splitting switching the loss distribution (SSLD) PWM which was proposed in [12]. Some of them, like PWM2 have already shown very high efficiency for the H-ANPC in the inverter mode of operation and high modulation index [3]. For others an application to an H-ANPC has not yet been investigated. The focus points of the comparison will be the temperature distributions, efficiency and the total harmonic distortion (THD) of the voltage, considering different operating conditions.

The structure of the paper is as follows. In the Section II the working principle and implementation of the four modulation strategies are presented. Afterwards, analysis of the thermal distribution, efficiency and harmonic distortion of the output voltage for the strategies is conducted in Section III. In Section IV the temperature distribution of the PWM2 strategy is validated on an open module 3-level H-ANPC prototype. Future work and conclusions are given in the final section.

## II. CONTROL STRATEGIES

Four different control strategies will be used to control the H-ANPC. The difference between the control strategies is in the way they utilize the 8 possible switching states available for each leg of the ANPC topology [13]. From the 8 switching states, 4 will connect the leg output to the neutral point (0L1, 0L2, 0U1, 0U2), 2 will connect to the positive DC-link voltage (p1, p2) and 2 to the negative (n1, n2) as shown in Table I. While selecting the control strategies, the PWM strategies, which do not fit the hybrid configuration from Fig. 1, were eliminated from the selection. Those strategies would for example switch the SiC devices with 50 Hz frequency and the Si devices with much higher frequency resulting in high switching losses (see PWM1 and modifications in [10], [11], [13], [14]).

### A. PWM2 algorithm

The first control strategy PWM2 is using two phase and amplitude shifted carriers to generate the PWM signals. As shown in [3] by using this algorithm, the inner devices are switched with the carrier frequency, while the other 4 devices are switching with much lower frequency. The generation of the switching signals is shown in Fig. 3a for the case when the reference signal is positive and in Fig. 3b for the case when the reference signal is negative. The duty cycle of the inner device $T_2$ is equal to the reference signal, while the outer device $T_1$ and clamping device $T_6$ are turned on the whole half cycle. Switching signals for the devices $T_3, T_4$ and $T_5$ are obtained by inverting the control signals of $T_2, T_1$ and $T_5$. This makes the PWM2 algorithm implementation to be the simplest algorithm which is evaluated in this paper.

### B. SSLD PWM algorithm

The next control strategy, SSLD PWM was developed by modifying the PWM2 to achieve a better loss distribution [12]. The transition from zero voltage level to $+V_{dc}/2$ or $-V_{dc}/2$ is the same as in the PWM algorithm. The difference is found in the introduction of a short intervals $0_{+out}$ and $0_{-out}$ after the transition from $+V_{dc}/2$ voltage level to zero voltage and $-V_{dc}/2$ voltage level to zero voltage, where both inner devices $(T_2, T_3)$ are conducting at the same time. The generated switching signals are shown in Fig. 4. It can be observed that for the SSLD PWM algorithm, control signals for the switches $T_3, T_4$ are no longer obtained by inverting the control signals of $T_2, T_1$.

### C. PWM3 algorithm

The third control strategy is PWM3 or also called double frequency PWM [11]. This strategy is using two phase shifted carriers. Due to the fact that the reference waveform has two intersections with the carrier signal during one switching period, the natural doubling of the switching frequency is obtained. In Fig. 5a and Fig. 5b the generation of the switching signals for positive reference value and the negative reference value can be observed. Compared to the PWM2 it can be noticed that PWM3 is using all 4 different switching combinations (0U2, 0L1, 0L2, 0U1) to obtain the zero voltage level. Different zero voltage vectors are used for the period of positive reference value and different for the negative reference value. The transitions from zero voltage level to $+V_{DC}/2$ or vice versa are arranged so that only one switch changes the state. The same applies also for transitions from zero
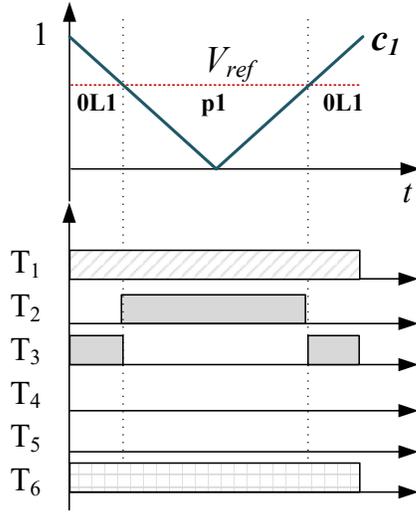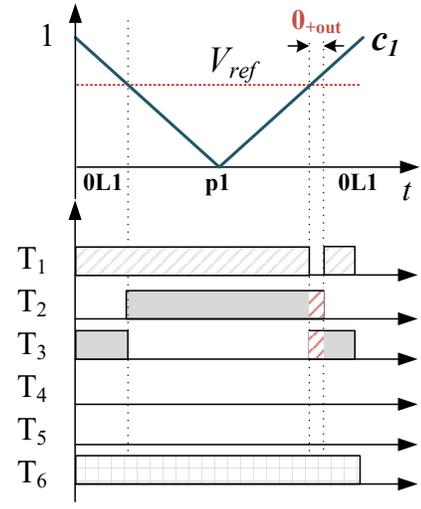
(a) For positive reference signal value.
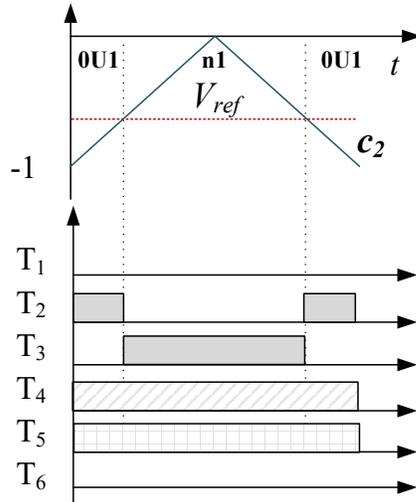


(b) For negative reference signal value.

Fig. 3: Generation of the switching signals for the three level ANPC converter using the PWM2 algorithm. $c_1, c_2$ are carrier signals.



(a) For positive reference signal value.



(b) For negative reference signal value.

Fig. 4: Generation of the switching signals for the three level ANPC converter using the SSLD algorithm. $c_1, c_2$ are carrier signals.
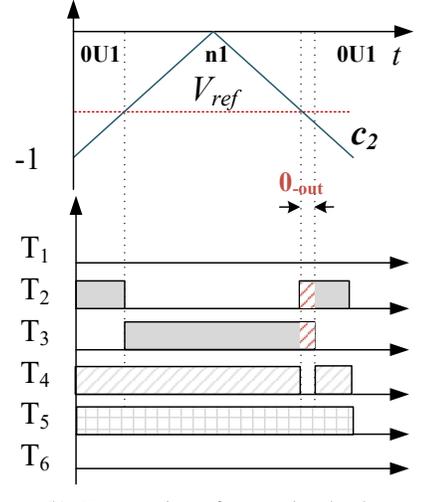
voltage level to $-V_{DC}/2$. This ensures a minimization of the switching losses. It can also be detected that for the PWM3 the switching signal for switch $T_4$ is no longer equal to the inverted switching signal of $T_1$ like in the PWM2 algorithm. Moreover, all devices of the ANPC converter are now operated as high frequency switches.

*D. LBC algorithm*

The fourth strategy is focusing on balancing the thermal stress of the inner and outer devices of the ANPC converter. It requires a more advanced implementation as it is using the device temperatures to select the correct switching combination, which will produce the junction temperature balance of the most stressed devices [1]. The temperature feedback can be obtained either by using a thermal model of the devices or directly by sensing the device temperatures. In Fig. 6 a required controller scheme is shown. The LBC

algorithm is using a look up table to select one of the four zero voltage switching combinations. As input variables the control algorithm requires the device junction temperatures $(T_1, T_2, T_3, T_4, D_1, D_2, D_3, D_4)$, commutation type and the converter output current direction. The look up table that is used for selecting the most suitable zero voltage switching combination is explained in more detail in [1].

One more control algorithm that could potentially be implemented is the adjustable losses distribution proposed in [15]. However, the strategy requires finding the correct stress-out/stress-in interval ratio to obtain the balance, which would just like the LBC algorithm require a temperature feedback.

## III. THERMAL DISTRIBUTION, EFFICIENCY AND THD ANALYSIS

For the analysis of the presented modulation strategies for the H-ANPC converter, three features are compared: thermal

(a) For positive reference signal value.



(b) For negative reference signal value.
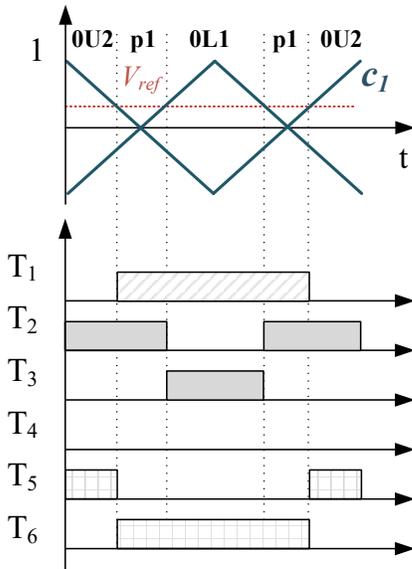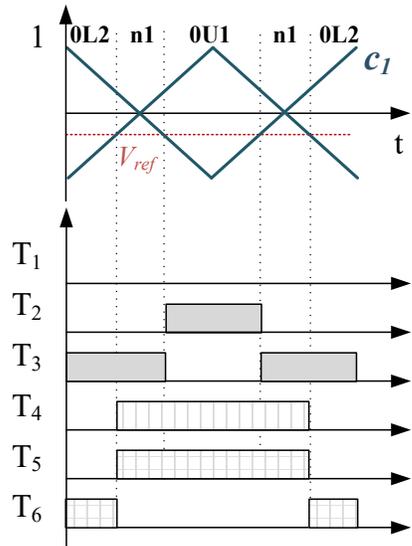
Fig. 5: Generation of the switching signals for the three level ANPC converter using the PWM3 algorithm. $c_1, c_2$ are carrier signals.

distribution, efficiency and total harmonic distortion. For this purpose, a simulation model of the converter system shown in Fig. 2 was created using Plecs Blockset and semiconductor device data sheets. The losses are calculated in Plecs by using a look-up table. The look-up table is fed with the information about conduction and switching losses from the device data sheets. Afterwards the losses are used as an input to a thermal network, which is based on the Foster model. The parameters of the converter system model are summarized in Table II.

### A. Thermal distribution

The thermal distribution is first analysed considering power flow to the load (inverter mode). As shown in Figs. 7a and
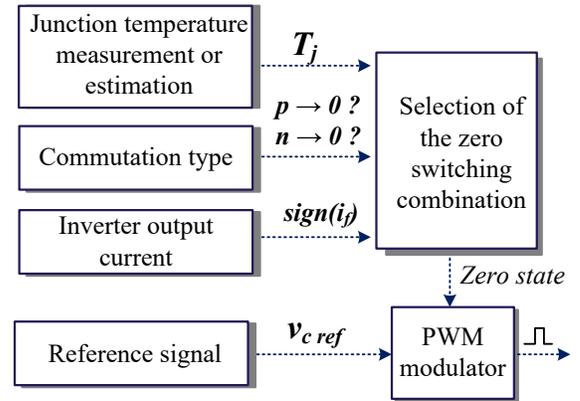


Fig. 6: Generation of the switching signals for the three level ANPC converter using the LBC algorithm.

TABLE II: System parameters.

| Parameter | Value |
|---|---|
| DC-link voltage ($V_{dc}$) | 700 V |
| Output filter ($C_f, L_f$) | 15 $\mu$F, 2.4 mH |
| Nominal power | 37 kW |
| Switching frequency | 32 kHz |
| Modulation index | 1, 0.5 |
| Power factor | 1, -1 |

7b, PWM2 presents lower temperatures in the outer devices for both modulation indexes (MI), due to the lower switching frequency. PWM3, in turn, shows a better balancing between internal and external devices and therefore, also a reduced temperature of the most stressed device. Considering the thermal balancing, LBC achieves the best performance at MI = 1, due to its closed-loop solution, yet higher losses due to the higher switching frequency of the external IGBT devices ($T_1, T_4$). The SSLD PWM, however, has the worst thermal distribution and, consequently, the highest thermal stress under inverter mode. This is due to the fact that by introducing the sharing of switching losses between the inner and outer device while operating at a high switching frequency, the outer device was put under too high switching stress. In the rectifier mode this effect was not present due to the low utilization of the outer devices. Another interesting point is that LBC does not achieve a perfect balancing for reduced modulation index even with a temperature feedback. In this structure, the body diode is used, which affects the MOSFET temperature and, consequently, the thermal distribution. Therefore, in order to achieve a perfect balancing in H-ANPC converters a modification on the traditional LBC algorithm is required [1].

The thermal balancing results for the H-ANPC converter operating rectifier mode are shown in Figs. 8a and 8b. As demonstrated, the lower switching frequency of the outer devices is also effective in this working condition, and PWM2 has the lowest thermal stress among the compared strategies. In this condition, the SSLD PWM has shown the second best thermal performance, whereby its highest thermal stress

TABLE III: Maximum junction temperature and temperature unbalance for different control algorithms, modulation indexes and operation modes ($\Delta T_{jT2,T1} = T_{jT2} - T_{jT1}, \Delta T_{jT2,D1} = T_{jT2} - T_{jD1}$).

| | Inverter mode | | | | Rectifier mode | | | |
|---|---|---|---|---|---|---|---|---|
| | MI = 1 | | MI = 0.5 | | MI = 1 | | MI = 0.5 | |
| Algorithm | $T_{jmax}$ (°C) | $\Delta T_{jT2,T1}$ (°C) | $T_{jmax}$(°C) | $\Delta T_{jT2,T1}$ (°C) | $T_{jmax}$(°C) | $\Delta T_{jT2,D1}$ (°C) | $T_{jmax}$(°C) | $\Delta T_{jT2,D1}$ (°C) |
| PWM 2 | 109.7 | **11.3** | 124.4 | **13.9** | 116.1 | **8.6** | 97.8 | **13.6** |
| PWM 3 | 114 | -2.5 | 118.9 | 7.2 | **126.2** | 2.7 | **115.4** | 11.8 |
| SSLD | **125.9** | -3.8 | **136.5** | 13.6 | 123.8 | 0.4 | 104.8 | 7.3 |
| LBC | 114 | 0 | 135.7 | 5.7 | 120 | 5.7 | 108 | 11 |



(a) MI = 1, $cos \phi = 1$.
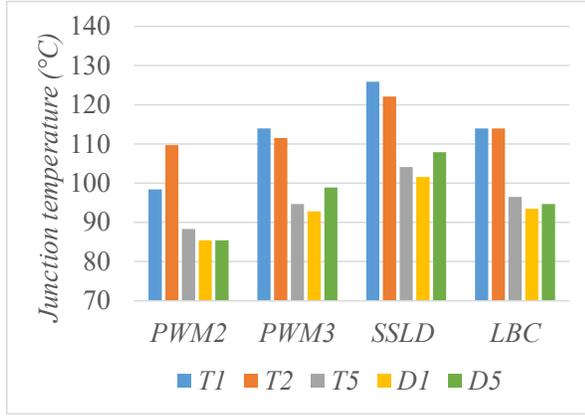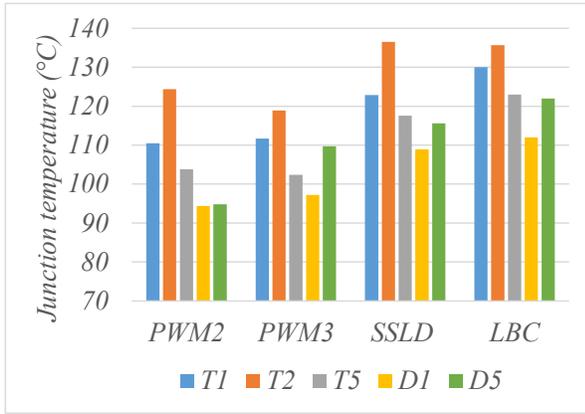


(b) MI = 0.5, $cos \phi = 1$.

Fig. 7: Thermal analysis for the H-ANPC converter considering different modulation strategies and modulation indexes for power flow to the load (inverter mode).



(a) MI = 1, $cos \phi = -1$.



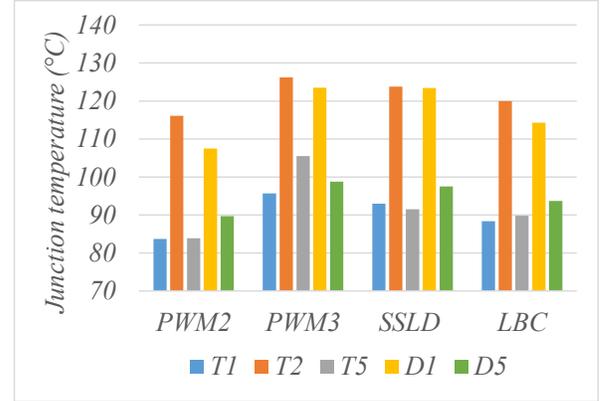(b) MI = 0.5, $cos \phi = -1$

Fig. 8: Thermal analysis for the H-ANPC converter considering different modulation strategies and modulation indexes for reverse power flow (rectifier mode).
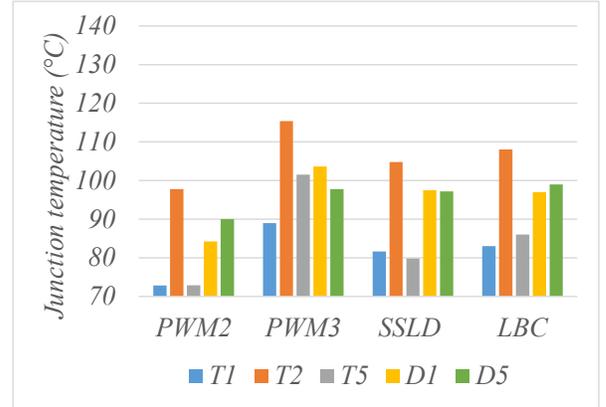
is smaller than PWM3 and LBC. Overview of the thermal distribution for all control algorithms in different operating conditions is given in Table. III.

### B. Efficiency and THD analysis

The total harmonic distortion and efficiency analysis are shown in Fig. 9. As it can be seen, PWM2 shows the best efficiency and most reduced THD due to the opt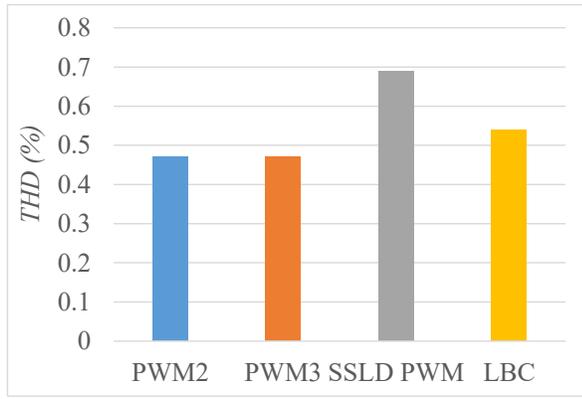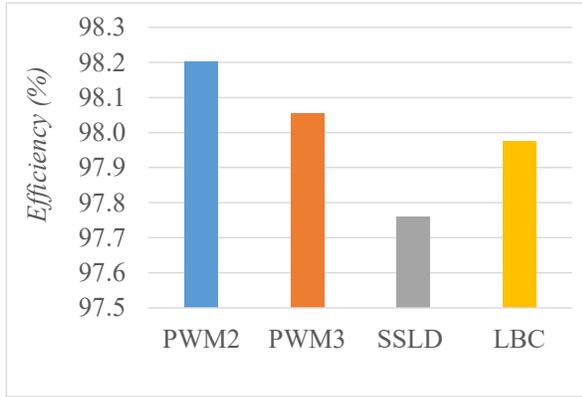imum switching frequency distribution. In the same way, PWM3 also demonstrates good efficiency and reduced THD for H-ANPC converters. The lowest score both in efficiency and harmonic distortion was obtained for the SSLD PWM, which was expected after the thermal distribution showed the highest device junction temperatures for the inverter mode. Thus, for the H-ANPC topology in terms of efficiency and harmonic distortion, PWM2 is the best choice. However, it needs to be mentioned that the PWM3 due the natural doubling of the switching frequency was used at a two times lower
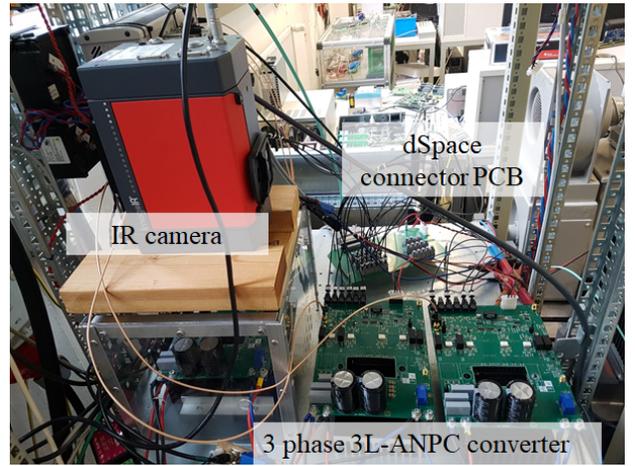
(a) Voltage THD.



(b) Converter efficiency.

Fig. 9: Total harmonic distortion and efficiency analysis for different modulations, MI = 1 and $cos \phi = 1$.



(a) Prototype with IR camera used for recording the junction temperatures.



(b) IR snapshot of the one phase ANPC open module using the PWM2 algorithm ($i_o$=35 A, $V_{dc}$=250V).

Fig. 10: Experimental set-up for validation of control strategies for hybrid ANPC converter.

switching frequency to make a fair comparison of the harmonic distribution with the PWM2 algorithm.
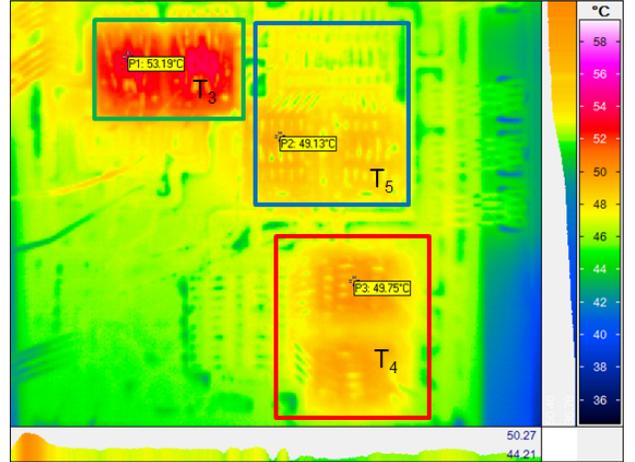
## IV. EXPERIMENTAL VALIDATION

The experimental validation of the PWM2 algorithm, which showed the highest efficiency and lowest harmonic distortion, will be performed on a three level H-ANPC prototype as shown in Fig. 10a. For the measurements of the device temperatures for single phase module of the H-ANPC, a high resolution Ifratec ImageIR 8300 camera was used [16]. The control algorithm is implemented in the dSpace MicroLabBox DS1202 control platform. A connector board is used to interface the gate signals coming from control platform to the optic fibre cables connected to the converter board. In order for the device temperatures to reach steady state, the IR snapshot was performed after 10 minutes of the converter operation.

In Fig. 10b an IR snaphot of the devices $T_3, T_4$ and $T_5$ can be seen. As shown in the simulations, the hottest device is the SiC MOSFET ($T_3$), which is switching with 32 kHz. 5° difference in junction temperature can be observed between the inner and outer devices. In terms of utilizing the advantages of topology devices, the PWM2 strategy is taking advantage of the good high switching frequency characteristics of SiC devices. However in terms of thermal distribution there exist

an unbalance in the junction temperatures of the inner and outer devices. A temperature difference of 5° can have a high impact on the expected lifetime of the devices as shown in [17].

## V. CONCLUSION

The comparison of the four different modulation strategies for H-ANPC showed that PWM2 modulation will produce the lowest losses, provide the highest efficiency and lowest voltage THD for both inverter and rectifier mode and high and medium modulation indexes. However, unbalanced loss distribution is one of the PWM2 disadvantages. This was also confirmed in the thermal measurements of the H-ANPC open module under inverter mode. On the other hand, PWM3 has a much better stress distribution balance than PWM2. A perfect balance of the inner and outer device junction temperatures is achieved using the LBC algorithm in the case of the inverter mode and high modulation index. However, a perfect balancing is not

achieved for a lower modulation index. SSLD PWM did not perform well for inverter mode.

As the obtained results showed that a single PWM modulation did not provide a balanced distribution in all converter operation points, a combination of the analysed PWM modulations could be used according to the operating point to improve the balance.

## REFERENCES

[1] T. Bruckner, S. Bernet, and H. Guldner, "The active NPC converter and its loss-balancing control," *IEEE Trans. Ind. Electron.*, vol. 52, no. 3, pp. 855–868, 2005.

[2] J. Rodriguez, S. Bernet, P. K. Steimer, and I. E. Lizama, "A survey on neutral-point-clamped inverters," *IEEE Trans. Ind. Electron.*, vol. 57, no. 7, pp. 2219–2230, 2010.

[3] Q. Guan, C. Li, Y. Zhang, S. Wang, D. D. Xu, W. Li, and H. Ma, "An extremely high efficient three-level active neutral-point-clamped converter comprising SiC and si hybrid power stages," *IEEE Trans. Power Electron.*, vol. 33, no. 10, pp. 8341–8352, 2018.

[4] M. Chen, T. Zhu, D. Pan, H. Wang, X. Wang, and F. Blaabjerg, "Loss analysis of SiC-based three-level active neutral-point-clamped inverters under different modulation schemes," in *Proc. of IEEE 9th Int. Power Electron. and Motion Control Conf. (IPEMC2020-ECCE Asia)*, 2020, pp. 971–978.

[5] H. Wang, X. Ma, and H. Sun, "Active neutral-point-clamped (ANPC) three-level converter for high-power applications with optimized pwm strategy," in *Proc. of Int. Exhib. and Conf. for Power Electron., Intelligent Motion, Renewable Energy and Energy Management (PCIM Asia)*, 2020, pp. 1–8.

[6] L. Zhang, X. Lou, C. Li, F. Wu, Y. Gu, G. Chen, and D. Xu, "Evaluation of different Si/SiC hybrid three-level active NPC inverters for high power density," *IEEE Trans. Power Electron.*, vol. 35, no. 8, pp. 8224–8236, 2020.

[7] D. Barater, C. Concari, G. Buticchi, E. Gurpinar, D. De, and A. Castellazzi, "Performance evaluation of a three-level ANPC photovoltaic grid-connected inverter with 650-v SiC devices and optimized PWM," *IEEE Trans. Ind. Appl.*, vol. 52, no. 3, pp. 2475–2485, 2016.

[8] L. Zhang, G. Chen, X. Yang, F. Zhao, Y. Gu, and Y. Xing, "An improved modulation strategy for "SiC+Si" hybrid five-level active NPC inverters," in *Proc. of IEEE 28th Int. Symp. on Ind. Electron.(ISIE)*, 2019, pp. 758–763.

[9] C. Li, R. Lu, W. Li, and Y. Wang, "Space vector modulation for SiC si hybrid active neutral point clamped converter," in *Proc. of IEEE Int. Power Electron. and Appl. Conf. and Expo. (PEAC)*, 2018, pp. 1–6.

[10] J. He, D. Zhang, and D. Pan, "PWM strategy for mw-scale "SiC+Si" active NPC converter in electric aircraft propulsion applications," *IEEE Tran. Ind. Appl.*, 2020, Early Access.

[11] D. Floricau, E. Floricau, and M. Dumitrescu, "Natural doubling of the apparent switching frequency using three-level ANPC converter," in *Proc. of Int. School on Nonsinusoidal Currents and Compensation*, 2008, pp. 1–6.

[12] G. Zhang, Y. Yang, F. Iannuzzo, K. Li, F. Blaabjerg, and H. Xu, "Loss distribution analysis of three-level active neutral-point-clamped (3L-ANPC) converter with different PWM strategies," in *Proc. of IEEE 2nd Annual Southern Power Electron. Conf. (SPEC)*, 2016, pp. 1–6.

[13] M. Novak, V. Šunde, N. Čobanov, and Z. Jakopović, "Semiconductor loss distribution evaluation for three level ANPC converter using different modulation strategies," in *Proc. of 19th Int. Conf. on El. Drives and Power Electron. (EDPE)*, 2017, pp. 170–177.

[14] Y. Jiao and F. C. Lee, "New modulation scheme for three-level active neutral-point-clamped converter with loss and stress reduction," *IEEE Trans. Ind. Electron.*, vol. 62, no. 9, pp. 5468–5479, 2015.

[15] L. Ma, T. Kerekes, P. Rodriguez, X. Jin, R. Teodorescu, and M. Liserre, "A new PWM strategy for grid-connected half-bridge active npc converters with losses distribution balancing mechanism," *IEEE Trans. Power Electron.*, vol. 30, no. 9, pp. 5331–5340, 2015.

[16] (2019) Ifratec ImageIR 8300 specifications. [Online]. Available: https://www.infratec.eu/thermography/infrared-camera/imageir-8300/

[17] M. Novak, V. Ferreira, M. Andresen, T. Dragicevic, F. Blaabjerg, and M. Liserre, "FS-MPC based thermal stress balancing and reliability analysis for NPC converters," *IEEE Open Journal of Power Electron.*, vol. 2, pp. 124–137, 2021.